SARCOIDOSIS VASCULITIS AND DIFFUSE LUNG DISEASES 2025; 42 (2): 16188 DOI: 10.36141/svdld.v42i2.16188 

# Non-invasive procedure in differential diagnosis of sarcoidosis and tuberculosis lymph nodes: Radiomic model of 18F-FDG PET-CT

*Damla Serçe Unat[1], Nursin Aguloğlu[2], Ömer Selim Unat[1], Ayşegül Aksu[3], Onur Fevzi Erer[4], Özer Özdemir[4], Gülru Polat[5]*

[1] Department of Pulmonology, Giresun Dr. Ali Menekşe Chest Diseases Hospital, Giresun, Turkey; [2] Department of Nuclear Medicine, Izmir Health Sciences University, Dr Suat Seren Chest Diseases and Chest Surgery Training and Research Hospital, Izmir, Turkey; [3] Department of Nuclear Medicine, Izmir Katip Celebi University, Faculty of Medicine, Izmir, Turkey; [4] Department of Pulmonology, Izmir Health Sciences University, Dr Suat Seren Chest Diseases and Chest Surgery Training and Research Hospital, Izmir, Turkey; [5] Department of Pulmonology, Izmir Health Sciences University, Izmir Faculty of Medicine, Izmir, Turkey

**Abstract.** *Background and aim:* Clinical and pathological features of two granulomatous diseases tuberculosis (TB) and sarcoidosis lymphadenopathy share similar properties. 18-F FDG Positron-Emission Tomography-Computed Tomography (18F-FDG PET-CT) is performed to discriminate two diseases. Even biopsy and culture via Endobronchial Ultrasonography (EBUS) sometimes did not get definite diagnosis. Radiomics can defined as high-throughput mining of radiological images. We aimed to investigate the role of radiomic analysis of these 18F-FDG PET/CT images in discrimination of TB and sarcoidosis. *Methods:* All patients with mediastinal LAP who underwent EBUS biopsy were screened for inclusion. Among these patients, patients who were diagnosed with TB or sarcoidosis by pathological and microbiological methods were included in the study. Radiomic model and clinicoradiomic models were formed AUC, sensitivity and specificity values of models obtained by logistic regression results were calculated. *Results:* 54 tuberculosis and 163 sarcoidosis lymph nodes were analyzed. Gender, GLCM_Correlation and GLCM_Energy features were found to be important prognostic factors in distinguishing between sarcoidosis and tuberculosis (p: 0.012, OR: 2.423 (1.215-4.830, 95% CI); p<0.001, OR: 5.400 (2.108-13.830, 95%) CI); p<0.001, OR: 3.335 (1.693-6.571, 95% CI; respectively). The p, AUC, sensitivity, and specificity values of the obtained clinicoradiomic model were calculated as <0.001, 0.762 (0.651-0.798, 95% CI), 59.5% and 81.5%, respectively. *Conclusions*: The model created with radiomics methods and clinical features gave significant results in distinguishing tuberculosis and sarcoidosis. This is promising for radiomic models that could replace invasive methods. It is expected that radiomic models will be used more in daily life in the future.

**Key words:** sarcoidosis, tuberculosis, 18F-FDG PET-CT, radiomic analysis

## Introduction

Sarcoidosis is a multisystem disease with a heterogeneous structure, characterized by granulomatous inflammation in specific organs. Tuberculosis, also another multisystem disease with granulomatous inflammation, (TB) is still the leading cause of death worldwide and gives a heavy burden to global health

Received: 8 July 2024
Accepted: 30 November 2024
**Correspondence:**
Damla Serçe Unat
Department of Pulmonology, Giresun Dr. Ali Menekşe Chest Diseases Hospital, Turkey
E-mail: sercedamla@gmail.com
ORCID: 0000-0003-4743-5469

systems. Two diseases are both important health problem globally. (1-5) In the differential diagnosis of these two disorders; clinical, laboratory, radiologic and even pathological methods are used. CT features of these two diseases may be distinguished by central low attenuation areas corresponding areas of caseous necrosis and peripheral rim enhancement that indicates granulation tissue. However, these signs can be seen in both diseases. Because of these challenges in the differential diagnosis of sarcoidosis lymph node and tuberculosis lymphadenitis, patients undergo invasive procedures to take samples from lymph nodes. Also in some cases, even though biopsy sample has taken differential diagnosis could not be possible. Some studies state that radiomic measurements may be helpful for discrimination of sarcoidosis and TB (6,7). Although endobronchial ultrasonography (EBUS) is frequently used to differentiate these two diseases, recent studies show that TB-PCR of EBUS guided biopsies have a sensitivity of %60 (8).Many pathophysiological similarities exist between TB and sarcoidosis. Pathological distinguishing can be tough in the absence of caseating granuloma and necrosis (9,10). Therefore, the use of non-invasive methods in differentiating these diseases can provide clinical benefit to physicians and comfort to patients. Accurate diagnosis is essential because treatment of sarcoidosis which is corticosteroid based and TB which is anti-mycobacterial are totally different (11). 18F-FDG PET/CT is sensitive in the diagnosis of sarcoidosis especially for the lymph nodes, but specificity is an obstacle for 18F-FDG PET/CT usage (4,12,13). Emerging technologies such as artificial intelligence and radiomics may be helpful for increasing the diagnostic accuracy of 18F-FDG PET/CT. Radiomics, is a new and breakthrough method that uses large numbers of images and analyzes those images. It has been proved to be functional for determining the emphysema, detecting the lung cancer and diagnosing the interstitial lung diseases (14). In this study, we evaluated the 18F-FDG PET/CT images of patients who had diagnosis of Sarcoidosis or TB. We aimed to investigate the role of radiomic analysis of these 18F-FDG PET/CT images in discrimination of these two diseases. We compared the radiomic model created by radiomic analysis with the definitive pathological or microbiological diagnosis.

## Materials and methods

### *Patient selection*

The data of patients diagnosed with sarcoidosis or tuberculosis at a tertiary referral chest diseases hospital between 2016-2019 years, were analyzed retrospectively (Figure 1). The study was single

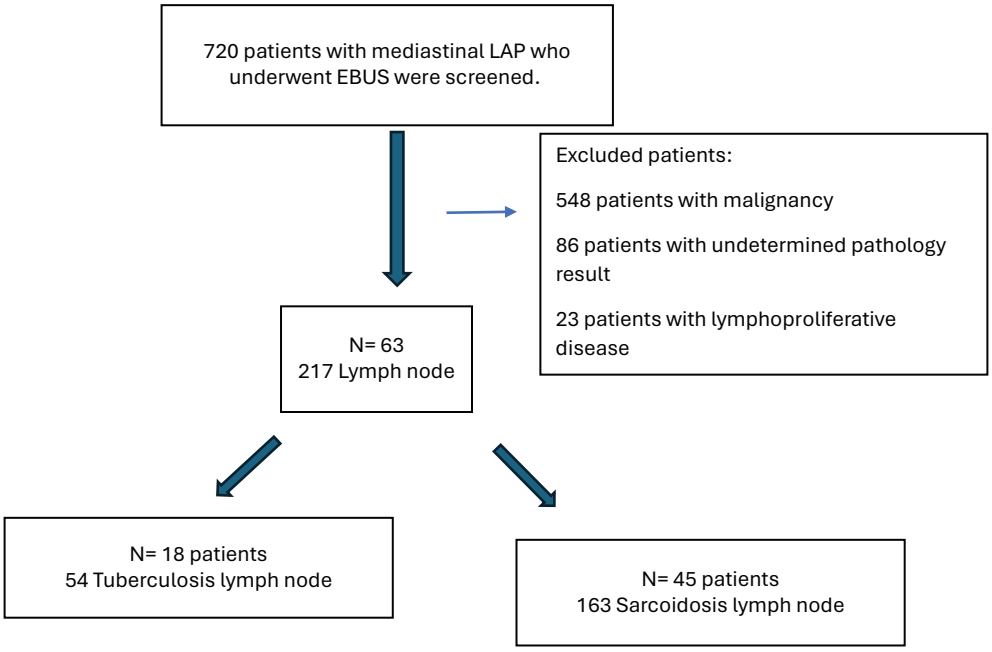


**Figure 1.** Identification of the patient population.

centered and started after the approval of the local Ethics Committee, dated 07.04.2023, and numbered 2023/ 37-37. All patients with mediastinal LAP who underwent EBUS biopsy, aged 18-90 years, and who were admitted to our hospital between 2016 and 2023, were screened for inclusion. Among these patients, patients who were diagnosed with TB or sarcoidosis by pathological and microbiological methods were included in the study.

*PET/CT protocol*

Imaging was performed on the Philips Gemini TF 16-slice combined PET/CT scanner and the same scanner was used for all patients. Following a minimum of 6 hours of fasting (blood glucose concentrations <150 mg/dl), 8–15 mCi 18F-FDG (2.5 MBq/kg body weight) was administered intravenously as defined in the European Nuclear Medicine Association (EANM) guidelines version 2.0 (15). The time between intravenous injection and scans was 60±5 minutes. The patients received no intravenous contrast agent. First CT images (140 kV, 100 mAs, 5-mm sections) and then PET images were acquired. Attenuation-corrected emission data were obtained using non-contrast enhanced data, extrapolated to 511 keV. PET images were acquired through emission scanning for 1.5 min per bed position, and a whole-body scan from the skull vertex to the proximal thigh using 9 or 10 bed positions. The images were reconstructed with iterative algorithms over a 128x128 matrix. The images were reconstructed using a 3D row-action maximum likelihood algorithm (RAMLA; two iterations, relaxation parameter 0.05, 5 mm full-width at half-maximum 3D gaussian postfiltering, 4×4×4 mm voxels).

*18F-FDG PET/CT Texture-Volumetric analysis*

The images of the patients were evaluated using LIFEx software (LIFEx, Orsay, France) (16). 18F-FDG PET/CT image of the patient in DICOM format was transferred to the software. Lymph node related region was evaluated semi-automatically by a nuclear medicine physician with 10 years of PET/CT experience using a 41% threshold on 18F-FDG PET/CT hybrid images. Texture characteristics of the lesions were obtained. Conventional SUV parameters, histogram and shape parameters were obtained. In further textural analysis, gray-level co-occurrence matrix (GLCM), gray-level run length matrix (GLRLM), neighborhood gray-level different matrix (NGLDM), and gray-level zone length matrix (GLZLM) parameters were measured. These features are summarized in Table 1. CT imaging has been used to acquire attenuated PET images only. CT data was not used in texture analysis.

*Statistics*

The data were analyzed using IBM SPSS 22 software. A p value less than 0.05 was considered as statistically significant. Descriptive data were

**Table 1.** Definition of parameters evaluated including conventional and advanced metabolic indices, shape features and radiomic texture features.

| Index | Matrix | Parameter |
|---|---|---|
| Conventional indices | | $SUV_{min}$, $SUV_{mean}$, $SUV_{max}$, $SUV_{peak}$, $SUV_{Std}$ |
| Volumetric indices | | MTV, TLG |
| Radiomic Texture features | GLCM | homogeneity, energy, contrast, correlation, entropy, dissimilarity |
| | NGLDM | coarseness, contrast, busyness |
| | GLRLM | SRE, LRE, LGRE, HGRE, SRLGE, SRHGE, LRLGE, LRHGE, GLNU, RLNU, RP |
| | GLZLM | SZE, LZE, LGZE, HGZE, SZLGE, SZHGE, LZLGE, LZHGE, GLNU, ZLNU, ZP |
| Shape features | | Sphericity, Surface, Compacity |

*Abbreviations:* SUV, standard uptake value; TLG, total lesion glycolysis; MTV, metabolic tumor volume,; GLCM, gray-level co-occurrence matrix; NGLDM, neighborhood gray-level different matrix; GLRLM, gray-level run-length matrix; GLZLM, gray level zone-length matrix; SRE, short-run emphasis; LRE, long-run emphasis; LGRE, low gray-level run emphasis; HGRE, high gray-level run emphasis, SRLGE, short-run low gray-level emphasis; SRGHE, short-run high gray-level emphasis; LRLGE, long-run row gray-level emphasis; LRHGE, long-run high gray-level emphasis; GLNU, gray-level non-uniformity; RLNU, run-length non-uniformity; RP, run percentage; SZE, short-zone emphasis; LZE, long-zone emphasis; LGZE, low gray-level zone emphasis; HGZE, high gray-level zone emphasis; SZLGE, short-zone low gray-level emphasis; SZHGE, short-zone high gray-level emphasis; LZLGE, long-zone low gray-level emphasis; LZHGE, long-zone high gray-level emphasis; ZLNU, zone-length non-uniformity; ZP, zone percentage

presented as mean, standard deviation, median and range values. Categorical variables were reported as frequencies with respective percentages. Spearman's correlation analysis was performed for correlation. Parameters which were not correlated with each other were selected. For pairwise comparisons, student t test or Mann Whitney U test was used for independent continuous variables, Chi square or Fisher exact test was used for categorical variables. Receiver operating characteristics (ROC) analysis was performed to determine the cutoff in the parameters obtained statistically significant, and the area under the curve (AUC) values were calculated. The cutoff was determined using the Youden Index to maximize specificity and sensitivity. Numerical data were dichotomized according to the determined cutoff value. The variables with statistically significant results were included in multivariate analysis, logistic regression was used in multivariate analysis and to build a model. A backward stepwise regression approach was used. Results of logistic regression are presented as odds ratios and corresponding 95% confidence intervals (CI). The AUC, sensitivity and specificity values of models obtained by logistic regression results were calculated. The multicollinearity between radiomic variables was assessed by using Variance Inflation Factor (VIF), that regards the standard error of the regression coefficients; a VIF factor greater than 2 was considered predictors for multicollinearity. VIF values were found to be below 2 for all variables.

## Results

Sixty-three patients – thirty-one of them (%49.2) were male with mean age of 62±13 (28-86) years were included in the study. Among these patients 18 (%28.6) had TB and 45 had sarcoidosis.

In all patients, the mean Hb value was 13.1±1.5, the mean WBC value was 7911.1±2562.3, the mean neutrophil value was 5079.4±2106.0, the mean lymphocyte value was 1982.5±1816.5, the mean eosinophil value was 242.9±188.1, the PLT value was 286.0 x $10^3$±90.1 x $10^3$. PLR mean was calculated as 181.9±102.2, NLR mean was 23.4±3.2. The total 217 lymph nodes were evaluated in EBUS diagnostic work-up. The relationship between lymph nodes diagnosed with sarcoidosis and tuberculosis and clinical-hemogram parameters are shown in Table 2.

There was statistically significant difference between sarcoidosis and tuberculosis groups among five texture parameters (Table 3).

All parameters showed intercorrelation except for GLCM_Correlation and GLCM_Energy. For this reason, the radiomic model was constructed using these two parameters. The cutoff value for GLCM_Correlation was determined as 0.300382. Sensitivity and specificity values at this cutoff value were determined as 40.5% and 88.9%, respectively. For GLCM_Energy, cutoff, sensitivity, and specificity values were calculated as 0.09264, 55.6% and 74.8%, respectively. When GLCM_Correlation and

**Table 2.** The relationship between lymph nodes diagnosed with sarcoidosis and tuberculosis and clinical-hemogram parameters.

| Variables | Tuberculosis (n=18) | Sarcoidosis (n=45) | p value |
|---|---|---|---|
| Age, mean±std | 63,2±12,8 | 61,3±13,2 | 0.61 |
| Gender, female (n) | 6 | 26 | 0.0.56 |
| Lymph Node (n)<br>Gender, female (n) | 54<br>19 | 163<br>91 | **0.009** |
| Hemoglobin mean±std (gr/ dL) | 13.0±1.7 | 13.1±1.4 | 0.87 |
| WBC, mean±std ( /μL) | 8533.3±2782.3 | 7811.1±2464.1 | 0.34 |
| Lymphocyte (/μL) (IQR 25-75) | 1700 (1540-2170) | 1800 (1400-2671) | 0.82 |
| Neutrophil mean±std (/μL) | 5600±2026.3 | 5013,3±2214.3 | 0.32 |
| Platelet ($10^3$/μL) (IQR 25-75) | 292.2±99.1 | 283.5± 87.4 | 0.74 |
| Eosinophil (/μL) (IQR 25-75) | 200 (143-345) | 200 (186-297) | 0.93 |
| PLR (IQR 25-75) | 177.2 (135-201) | 158.3 (152-20) | 0.96 |
| NLR (IQR 25-75) | 3.2 (2.7-3.5) | 2.5 (2.4-4.8) | 0.38 |

*Abbreviations:* WBC: White blood cell PLR: Platelet/ lymphocyte ratio NLR: Neutrophil / platelet ratio

GLCM_Energy features were analyzed by logistic regression, it was seen that both GLCM_Energy (p<0.001, OR: p: 0.001, OR: 3.389, 1.741-6.596, 95% CI) and GLCM_Correlation (p: 0.001, OR: 4.949, 1.969-12.442, 95% CI) were found to be important diagnostic factors in distinguishing between sarcoidosis and tuberculosis. The cut-off value of radiomic model was 0.618. The p, AUC, sensitivity, and specificity values of the obtained radiomic model were calculated as <0.001, 0.724 (0.651-0.798, 95% CI), 82.8% and 48.1%, respectively. Positive predictive value (PPV) was 34.6%, negative predictive (NPV) was 89,4%, likelihood ratio + (LR+) was +1,60 and likelihood ratio - (LR-) was 0,36 (Figure 2). When gender, GLCM_Correlation and GLCM_Energy features were analyzed with logistic regression, it was seen that all 3 parameters (gender, p: 0.012, OR: 2.423 (1.215-4.830, 95% CI); GLCM_Correlation, p<0.001, OR: 5.400 (2.108-13.830, 95%) CI), GLCM_Energy, p<0.001, OR: 3.335 (1.693-6.571, 95% CI) were found to be important prognostic factors in distinguishing between sarcoidosis and tuberculosis. The cut-off value of radiomic model was 1.417. The p, AUC, sensitivity, and specificity values of the obtained clinicoradiomic model were calculated as <0.001, 0.762 (0.651-0.798, 95% CI), 59.5% and 81.5%, respectively. PPV was 90,7%, negative predictive (NPV) was 40%, likelihood ratio + (LR+) was +3,22 and likelihood ratio - (LR-) was 0,50 (Figure 2).

**Table 3.** Parameters showing significant differences between lymph nodes diagnosed with sarcoidosis and tuberculosis

| Textures | p value | AUC (95% CI) |
|---|---|---|
| GLCM_Energy | 0.038 | 0.594 (0.494-0.695) |
| GLCM_Correlation | 0.002 | 0.644 (0.564-0.724) |
| GLCM_Entropy log 10&2 | 0.038 | 0.594 (0.495-0.694) |
| GLRLM_RLNU | 0.025 | 0.602 (0.502-0.698) |
| GLZLM_GLNU | 0.027 | 0.600 (0.502-0.698) |

## Discussion

In our study we found that radiomic analyses of 18F-FDG PET/CT images of mediastinal lymph nodes can be helpful in distinguishing TB and sarcoidosis. This study indicates that gender,

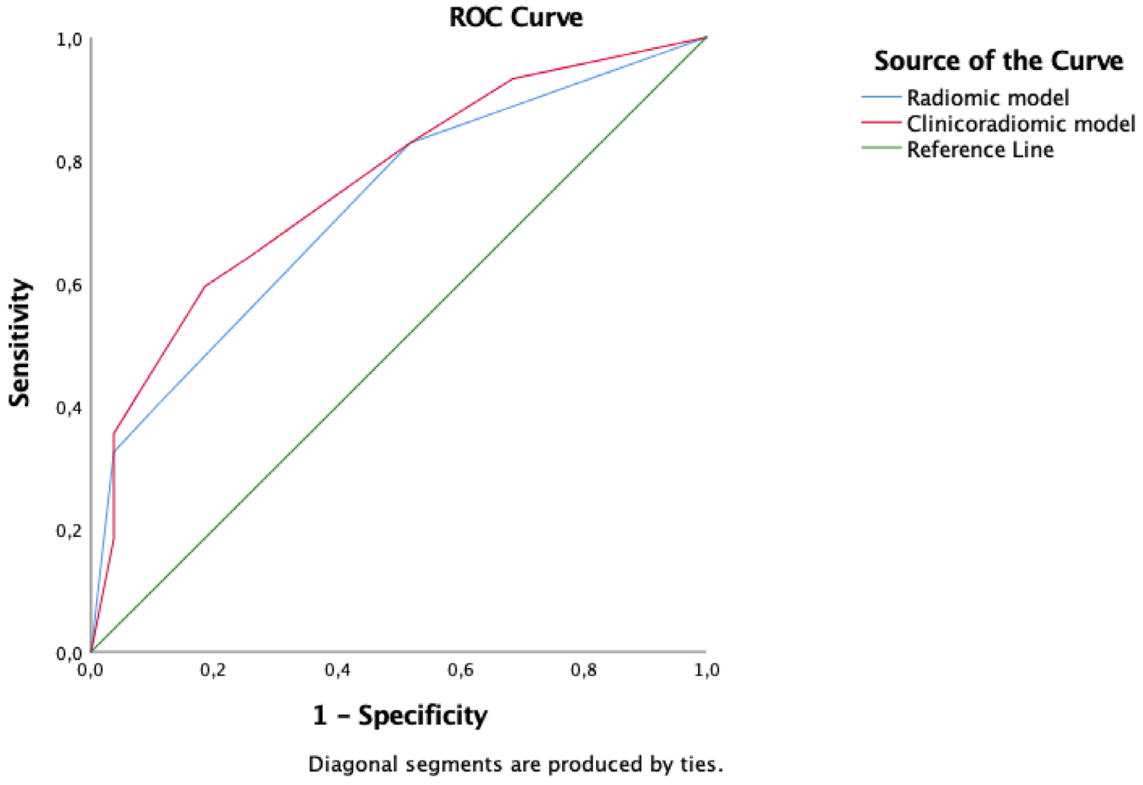


**Figure 2.** ROC curves of the models, radiomic model AUC: 0.724, clinicoradiomic model AUC: 0.761.

GLCM_Correlation and GLCM_Energy features are prominent tools in the differential diagnosis of TB and sarcoidosis. Radiomic model which formed by only radiomic parameters and clinicoradiomic model which combined by radiomic parameters and gender were both useful for discrimination of these two diseases. Differential diagnosis of TB and Sarcoidosis needs multimodal approach. There has been shown that combination of EBUS-fine needle aspiration biopsy (FNAB) and mycobacterial culture is the most accurate diagnostic method. But sometimes definite diagnosis may not be obtained even by EBUS-FNAB (17,18). 18- FDG PET-CT is used in the diagnosis and follow-up of both tuberculosis and sarcoidosis. Pulmonary tuberculoma nodules can be seen in hypermetabolic nodules in the PET-CT scan. Also, PET-CT can be extremely helpful in the diagnosis of extrapulmonary tuberculosis such as skeletal tuberculosis lesions. Apart from FDG, some tracers which are specific to tuberculosis can be used in the complicated cases. But these tracers are not routinely used. Du et al compared 18F-FDG and 18F-Alfatide II (a tracer molecule that targets integrin αVβ3 on the surface of cancer cells and neovascularized epithelial cells) in distinguishing tuberculosis lymphadenopathy and malignant lymphadenopathy. In that study, they found that 18F-Alfatide II PET-CT is more accurate than 18F-FDG PET-CT in terms of discrimination of malignant and tuberculosis lymphadenopathy (19). However, since tracer molecules are difficult and costly to access, these methods cannot be used in daily practice. For these reasons, strengthening routine examinations with new technologies may be more effective in terms of cost and usability. In our study, we performed radiomic analysis based on 18-FDG PET-CT parameters, which is a routine PET-CT application.

Sarcoidosis has some certain features in the PET-CT. In thoracic sarcoidosis the most common PET-CT pattern is symmetrically low grade FDG-uptake bilateral hilar lymphadenopathy. In addition to lymph nodes involvement, PET-CT may be used in diagnosis and follow-up of parenchymal involvement of the sarcoidosis. Because of the avid nature of granulomatous tissues to the FDG, PET-CT can be used in the follow-up of tuberculosis and sarcoidosis. It is assumed that if there is good response to the treatment, there will be decrease in the FDG uptake (20–22). Models formed by radiomic analysis and deep learning methods can be helpful in the diagnosis of mediastinal lymphadenopathy. Although there is no study about the role of radiomics in discriminating tuberculosis and sarcoidosis in our study, Ma X. et al. suggested that CT-based radiomics models are more successful than radiologist opinion in determining malignant and benign lymphadenopathy (23). Radiomic analysis and machine-learning (ML) approaches were used in the differential diagnosis of sarcoidosis. In the study of Nakajo et al. analyzed the role of ML algorithms via 18F-FDG PET-CT to estimate the adverse clinical events (development of heart failure, arrhythmia). It has been found that ML algorithms especially random forest model, were useful for predicting adverse clinical events (24). Another study about this issue was compared radiomic model and physicians in differential diagnosis of sarcoidosis and lymphoma. In this study, authors encountered that diagnostic accuracy of radiomic models of 18F-FDG PET-CT were better or equivalent to the physicians. So, they concluded that radiomic models and ML approaches were useful tool in differentiating the sarcoidosis and lymphoma (25). Radiomics analyses were also studied in determining solitary malignant nodules of lung and Zhao et al suggested that combined model which integrates enhanced CT radiomic analysis and clinical properties is more accurate than pure radiomic model and radiologists. (AUC = 0.917, AUC=0.881, AUC = 0.611, respectively) (26). Likewise, in our study, clinicoradiomic model which formed by gender and radiomic textures were more accurate than radiomic model. Radiomic analyzes have been used quite frequently in the field of pulmonology recently. For instance, the radiomic model created by thorax CT-derived radiomic analysis was found to be effective in distinguishing pulmonary mucinous adenocarcinoma from pulmonary tuberculoma. In addition, the radiomic approach was found to be effective in the differential diagnosis of hamartoma and carcinoid tumor. (27,28). Also, radiomic analysis of pulmonary magnetic resonance in the pulmonary nodules is useful (29). Radiomic analyses are useful in certain areas of thoracic oncology such as differentiating benign and malign nodules, understanding the source of metastatic pulmonary nodule, or even estimating the prognosis. Shang et al applied radiomics methods in thoracic-CT and they showed that radiomics can be useful in determining the source of the metastatic nodule (colorectal cancer, breast cancer or renal carcinoma) (30). In the study of Zhang et al, they

showed that radiomic analysis is in the estimation of prognosis in malignant patients (31). CT-derived radiomics models are also used to distinguish infectious diseases. It has been observed that radiomics modeling is more accurate than the clinical model in distinguishing pulmonary echinococcus from pulmonary abscess (32). Although there are PET-CT findings for tuberculosis and sarcoidosis, it is difficult for clinicians to distinguish the cause of lymph adenopathy. We aim to distinguish sarcoidosis and tuberculosis lymph nodes by using PET-CT radiomic analysis as a non-invasive method. Our study has important strengths. Although there are some studies on PET-CT findings of sarcoidosis and infectious diseases, our study is the first to differentiate tuberculosis and sarcoidosis in mediastinal lymph nodes using PET-CT radiomic analysis. We combined radiomic and clinical parameters and formed a combined model. This is also another strength of our study. Our study has certain limitations. Firstly, this is a retrospective and single centered study. Also, we do not have studying and testing cohorts for the models. We used only one cohort in the comparison of these models. Radiomics can defined as high-throughput mining of radiological images. By this way it can provide more detailed information about tumor or lesion heterogeneity. In our study, we use radiomic analyses of PET-CT and we found that five texture parameters. With the model created using these five parameters, the differential diagnosis of sarcoidosis and tuberculosis lymph node could be made to a successful extent. The model created with radiomics methods and clinical features gave significant results in distinguishing tuberculosis and sarcoidosis. This is promising for radiomic models that could replace invasive methods such as EBUS. It is expected that radiomic models will be used more in daily life in the future.

**Conflict of interest:** Each author declares that he or she has no commercial associations (e.g. consultancies, stock ownership, equity interest, patent/licensing arrangement etc.) that might pose a conflict of interest in connection with the submitted article.

**Authors' contribution:** DSU made prominent contributions to the conception of work. DSU and OSU also made significant contributions to the collection of data and writing process. AA, NA and OSU made significant contributions to the interpretation of data and reviewed the paper. DSU and AA made important contributions to the interpretation and collection of data. OSU and GP played role in the writing and editing processes. OFE and OO made significant contributions to the collection of data. OFE and GP played vital role in the conception of work, interpretation of data and reviewing of paper. All authors have approved the submitted version of the manuscript.

## References


1. Global tuberculosis report 2022. Geneva: World Health organization; 2022. licence: cc bY-Nc-sa 3.0 iGo.
2. Visca D, Ong CWM, Tiberi S, et al. Tuberculosis and COVID-19 interaction: A review of biological, clinical and public health effects. Pulmonology. 2021 Mar;27(2):151–65.
3. Jonas DE, Riley SR, Lee LC, et al. Screening for Latent Tuberculosis Infection in Adults: Updated Evidence Report and Systematic Review for the US Preventive Services Task Force. JAMA. 2023 May;329(17):1495–509.
4. Keijsers RGM, Grutters JC. In Which Patients with Sarcoidosis Is FDG PET/CT Indicated? J Clin Med 2020, Vol 9, Page 890. 2020 Mar;9(3):890.
5. Belperio JA, Shaikh F, Abtin FG, et al. Diagnosis and Treatment of Pulmonary Sarcoidosis: A Review. JAMA. 2022 Mar;327(9):856–67.
6. Calandriello L, D'abronzo R, Pasciuto G, et al. Novelties in Imaging of Thoracic Sarcoidosis. J Clin Med 2021, Vol 10, Page 2222. 2021 May;10(11):2222.
7. Lee CU, Chong S, Choi HW, et al. Quantitative image analysis using chest computed tomography in the evaluation of lymph node involvement in pulmonary sarcoidosis and tuberculosis. PLoS One. 2018 Nov;13(11).
8. Mondoni M, Saderi L, Puci MV, et al. Xpert MTB/RIF in the Diagnosis of Mediastinal Tuberculous Lymphadenitis by Endoscopic Ultrasound-Guided Needle Aspiration Techniques: A Systematic Review and Meta-Analysis. Respiration. 2023 Mar;102(3):237–46.
9. Dubaniewicz A. Mycobacterial Heat Shock Proteins in Sarcoidosis and Tuberculosis. Int J Mol Sci 2023, Vol 24, Page 5084. 2023 Mar;24(6):5084.
10. Typiak M, Rękawiecki B, Rębała K, et al. Comparative Analysis of FCGR Gene Polymorphism in Pulmonary Sarcoidosis and Tuberculosis. Cells. 2023 May;12(9):1221.
11. Obi ON, Saketkoo LA, Russell AM, et al. Sarcoidosis: Updates on therapeutic drug trials and novel treatment approaches. Front Med. 2022 Oct;9:991783.
12. Papiris SA, Georgakopoulos A, Papaioannou AI, et al. Emerging phenotypes of sarcoidosis based on 18F-FDG PET/CT: a hierarchical cluster analysis. https://doi.org/101080/1747634820201684902. 2019 Feb;14(2):229–38.
13. Özütemiz C, Koksel Y, Froelich JW, et al. Comparison of the Effect of Three Different Dietary Modifications on Myocardial Suppression in 18F-FDG PET/CT Evaluation of Patients for Suspected Cardiac Sarcoidosis. J Nucl Med. 2021 Dec;62(12):1759–67.
14. Ryan SM, Fingerlin TE, et al. Radiomic measures from chest high-resolution computed tomography associated with lung function in sarcoidosis. Eur Respir J. 2019 Aug;54(2).
15. Boellaard R, Delgado-Bolton R, et al. FDG PET/CT: EANM procedure guidelines for tumour imaging: version 2.0. Eur J Nucl Med Mol Imaging [Internet]. 2015 Feb 1 [cited 2024 Feb 12];42(2): 328–54. Available from: https://pubmed.ncbi.nlm.nih.gov/25452219/
16. Nioche C, Orlhac F, Boughdad S, et al. LIFEx: A Freeware for Radiomic Feature Calculation in Multimodality Imaging to Accelerate Advances in the Characterization of Tumor Heterogeneity. Cancer Res [Internet]. 2018 Aug 15 [cited 2024 Feb 12];78(16):4786–9. Available from: https://pubmed.ncbi.nlm.nih.gov/29959149/
17. Fritscher-Ravens A, Ghanbari A, Topalidis T, et al. Granulomatous mediastinal adenopathy: can endoscopic ultrasound-guided fine-needle aspiration differentiate between tuberculosis and sarcoidosis? Endoscopy. 2011 Nov;43(11):955-61. doi: 10.1055/s-0031-1271110. Epub 2011 Aug 10. PMID: 21833904.

18. Kerget B, Afşin DE, Aksakal A. The role of systemic immune-inflammation index (SII) in the differential diagnosis of granulomatous and reactive LAP diagnosed by endobronchial ultrasonography: Evaluation of the systemic immune-inflammation index in sarcoidosis, tuberculosis and reactive lymphadenitis. Sarcoidosis Vasc Diffuse Lung Dis [Internet]. 2023 Sep. 13 [cited 2024 Nov. 29];40(3):e2023038. Available from: https://mattioli1885journals.com/index.php/sarcoidosis/article/view/14743
19. Du X, Zhang Y, Chen L, et al. Comparing the Differential Diagnostic Values of $^{18}$F-Alfatide II PET/CT between Tuberculosis and Lung Cancer Patients. Contrast Media Mol Imaging. 2018 Feb 19;2018:8194678. doi: 10.1155/2018/8194678. PMID: 29670497; PMCID: PMC5836463.
20. Kung BT, Seraj SM, Zadeh MZ, t al. An update on the role of 18F-FDG-PET/CT in major infectious and inflammatory diseases. Am J Nucl Med Mol Imaging [Internet]. 2019 [cited 2024 Feb 12];9(6):255. Available from: /pmc/articles/PMC6971480/
21. Vaidyanathan S, Patel CN, Scarsbrook AF, et al. FDG PET/CT in infection and inflammation--current and emerging clinical applications. Clin Radiol [Internet]. 2015 Jul 1 [cited 2024 Feb 12];70(7):787–800. Available from: https://pubmed.ncbi.nlm.nih.gov/25917543/
22. Xu B, Guan Z, Liu C, et al. Can multimodality imaging using 18F-FDG/18F-FLT PET/CT benefit the diagnosis and management of patients with pulmonary lesions? Eur J Nucl Med Mol Imaging [Internet]. 2011 Feb [cited 2024 Feb 12];38(2):285–92. Available from: https://pubmed.ncbi.nlm.nih.gov/20936411/
23. Ma X, Xia L, Chen J, et al. Development and validation of a deep learning signature for predicting lymph node metastasis in lung adenocarcinoma: comparison with radiomics signature and clinical-semantic model. Eur Radiol. 2023 Mar;33(3):1949-1962. doi: 10.1007/s00330-022-09153-z. Epub 2022 Sep 28. PMID: 36169691.
24. Nakajo M, Hirahara D, Jinguji M, et al. Machine learning approach using 18F-FDG-PET-radiomic features and the visibility of right ventricle 18F-FDG uptake for predicting clinical events in patients with cardiac sarcoidosis. Jpn J Radiol. 2024 Jul;42(7):744-52. doi: 10.1007/s11604-024-01546-y.
25. Lovinfosse P, Ferreira M, Withofs N, et al. Distinction of Lymphoma from Sarcoidosis on 18F-FDG PET/CT: Evaluation of Radiomics-Feature-Guided Machine Learning Versus Human Reader Performance. J Nucl Med. 2022 Dec;63(12):1933-40. doi: 10.2967/jnumed.121.263598.
26. Zhao W, Xiong Z, Jiang Y, et al. Radiomics based on enhanced CT for differentiating between pulmonary tuberculosis and pulmonary adenocarcinoma presenting as solid nodules or masses. J Cancer Res Clin Oncol. 2023 Jul;149(7):3395-408. doi: 10.1007/s00432-022-04256-y.
27. Zhang J, Hao L, Qi M, et al. Radiomics nomogram for preoperative differentiation of pulmonary mucinous adenocarcinoma from tuberculoma in solitary pulmonary solid nodules. BMC Cancer. 2023 Mar 21;23(1):261. doi: 10.1186/s12885-023-10734-4.
28. Yang X, Li C, Hou J, et al. Differentiating Peripherally Located Pulmonary Noncalcified Hamartoma From Carcinoid Using CT Radiomics Approaches. J Comput Assist Tomogr. 2023 May-Jun 01;47(3):402-11. doi: 10.1097/RCT.0000000000001414.
29. Zhou J, Wen Y, Ding R, et al. Radiomics signature based on robust features derived from diffusion data for differentiation between benign and malignant solitary pulmonary lesions. Cancer Imaging. 2024 Jan 22;24(1):14. doi: 10.1186/s40644-024-00660-4.
30. Shang H, Li J, Jiao T, et al. Differentiation of Lung Metastases Originated From Different Primary Tumors Using Radiomics Features Based on CT Imaging. Acad Radiol. 2023 Jan;30(1):40-6. doi: 10.1016/j.acra.2022.04.008.
31. Zhang R, Wei Y, Shi F, et al. The diagnostic and prognostic value of radiomics and deep learning technologies for patients with solid pulmonary nodules in chest CT images. BMC Cancer. 2022 Nov 1;22(1):1118. doi: 10.1186/s12885-022-10224-z.
32. Li Y, Yu Y, Liu Q, et al. A CT-based radiomics nomogram for the differentiation of pulmonary cystic echinococcosis from pulmonary abscess. Parasitol Res. 2022 Dec;121(12):3393-401. doi: 10.1007/s00436-022-07663-9.